# Polymorphism and Solidification Kinetics of the Binary System POS–SOS

**Ph. Rousset[b,*], M. Rappaz[a], and E. Minner[b]**

[a]Département des Matériaux, Ecole Polytechnique Fédérale de Lausanne, MX-G, CH-1015 Lausanne, Switzerland, and [b]Nestec S.A., Nestlé Research Center, 1000 Lausanne 26, Switzerland

**ABSTRACT:** As a first approach to modeling the crystallization behavior of cocoa butter, the binary system of its two major components, 1-palmitoyl-2-oleoyl-3-stearoyl-*sn*-glycerol (POS) and 1,3-distearoyl-2-oleoyl-*sn*-glycerol (SOS), was studied. Differential scanning calorimetry, coupled with polarized light microscopy, was used to determine the phase diagrams of the various polymorphic forms (the most metastable sub-α and α, intermediate δ and β′, and stable β). Associated theoretical phase diagrams were also built. The presence of a solid solution for β and the ideal behavior of α were confirmed. Kinetics of isothermal solidification as a function of temperature were studied for three compositions of the POS–SOS system. Results were displayed as time–temperature–transformation (TTT) diagrams and crystal morphology maps. Dependence of the crystallization kinetics on composition of the binary system was interpreted in terms of nucleation and growth mechanisms. The asymmetry of the POS molecule induces a slower growth rate of the mixture when the concentration of this triacylglycerol is increased. Solidification kinetics during continuous cooling were studied at various cooling rates for the system POS–SOS 25:75. Experimental results were compared with numerical predictions of a solidification model based upon TTT data and an additivity principle. The calculated and measured volume fractions of the different phases formed and times of onset and finish of the solidification were in good agreement.
*JAOCS 75*, 857–864 (1998).

**KEY WORDS:** Binary system, cocoa butter, crystallization, DSC, kinetics, polarized light microscopy, polymorphism, POS, SOS, triacylglycerol.

1-Palmitoyl-2-oleoyl-3-stearoyl-*sn*-glycerol (POS) and 1,3-distearoyl-2-oleoyl-*sn*-glycerol (SOS) are the two major components of cocoa butter. These products exhibit several polymorphic forms. Characteristics of the various crystalline forms of these pure triacylglycerols (TAG) (1–6), as well as their kinetic behavior (7–10), have been intensively studied. The extension of these studies to more complex mixtures is of particular interest for understanding the crystallization of a natural fat, such as cocoa butter. The binary system POS–SOS is a first step in this direction. A comprehensive review of the phase diagrams of TAG has been made by Rossel (11). Investigations done on the POS–SOS system by Wille and Lutton (12) showed a solid solution for the three phases observed, but there is some controversy about the existence of a eutectic for the β phase (13). Despite this, the most relevant diagram for this system, e.g., this measured by Wesdorp (6), confirmed the complete mixing behavior in the β phase. On the other hand, the less-stable phases of the POS–SOS system have not been completely identified and the kinetics of solidification were not characterized.

In the present study, differential scanning calorimetry (DSC) coupled with polarized light microscopy experiments was used to determine the phase diagrams of the various polymorphic forms in the POS–SOS system. The kinetics of isothermal crystallization are presented in the form of time–temperature–transformation (TTT) diagrams and microstructure maps. Evolution with composition of the mixtures POS–SOS was interpreted. Moreover continuous cooling experiments were compared with results from a solidification model.

## MATERIALS AND METHODS

*Experiments.* POS and SOS (purity at least 99%) were purchased from Larodan Fine Chemicals AB (Malmö, Sweden). Seven different compositions of the POS–SOS alloy were studied: 10:90, 25:75, 33:67, 50:50, 67:33, 75:25, and 90:10. They were prepared by accurately weighing the pure components and then mixing them thoroughly in a small glass pan at 100°C for several hours. The homogeneity of the binary mixtures was checked by gas chromatography.

The behavior of the binary system POS–SOS was investigated in a DSC Mettler FP900 instrument (Greifensee, Switzerland), which allows simultaneous calorimetric measurements and *in situ* microscopic observations under polarized light. For that purpose, the samples were placed in small glass pans, and formation of the solid phases was directly observed by transmission with a polarized-light microscope. Another instrument, a Perkin-Elmer (Norwalk, CT) DSC7, also was used for thermal measurements in classical aluminum pans. The mass of the DSC samples analyzed was between 1 and 2.5 mg. All isothermal solidification experiments were operated according to the following thermal path: first, the sample was kept at 100°C for 3 min to ensure a com-

*To whom correspondence should be addressed.
E-mail: Philippe.ROUSSET@chlsnr.nestrd.ch

pletely liquid state; then, it was rapidly cooled (50°C/min for the DSC7, 10°C/min for the FP900) to the desired temperature $T_{iso}$, at which crystallization was allowed to proceed. After complete solidification, the sample was heated at 2 or 5°C/min to measure the melting range (MR) and the latent heat of fusion for each solid phase formed. The MR was usually wide, and two superimposed melting peaks were observed. After deconvolution, the onset temperatures of these two peaks were interpreted as the solidus and liquidus temperatures. These measurements allowed identification of the phases by comparison with the values of the pure components (1–3,8). Unambiguous determination of phases on TAG binary mixtures can be accomplished by synchrotron radiation X-ray diffraction (14,15). Characteristics of the most stable phases were also determined after storing the solidified samples for several weeks at room temperature and then recording a DSC fusion curve at 2 or 5°C/min.

*Phase diagrams*. Thermodynamic models were used to analyze the experimental phase diagrams of the POS–SOS system. According to previous investigations (6), the liquid phase of the binary alloy can be approximated by an ideal solution. The free energy of the system is then simply given by the free energies of the two pure components, A and B, plus the configurational entropy:

$$G^l(T,X_A^l) = X_A^l G_A^l + (1 - X_A^l)G_B^l + RT\,[X_A^l \ln X_A^l + (1 - X_A^l)\ln(1 - X_A^l)] \quad [1]$$

where $G^l$ is the molar free energy of the liquid mixture, $G_A^l$, $G_B^l$ the molar free energies of pure elements *A* and *B*, respectively, $X_A^l$ the mole fraction of element *A* in the liquid, *T* the temperature of the system, and *R* the universal gas constant.

Two models were considered for the solid phases: the phase was supposed to be either an ideal solution like the liquid state, or a subregular solution (16). In the first case, an equation identical to Equation 1 was used with superscript "*l*" replaced by "*s*". In the second case, the free energy of the solid had an additional term, an excess free energy:

$$\Delta G_e^s = [\Omega_{BA} X_A^s + \Omega_{AB}(1 - X_A^s)]X_A^s (1 - X_A^s) \quad [2]$$

where $\Omega_{BA}$ and $\Omega_{AB}$ are interaction coefficients of the subregular model. If $\Omega_{BA} = \Omega_{AB}$, the model reduces to the regular solution approximation.

Setting the reference points $G_B^l = G_A^l = 0$, the free energies of the solid become:

$$G_A^s = \Delta G_A^{l->s} \approx \Delta H_f^A \frac{T_f^A - T}{T_f^A} \text{ and } G_B^s = \Delta G_B^{l->s} \approx \Delta H_f^B \frac{T_f^B - T}{T_f^B} \quad [3]$$

with $\Delta H_f^{A/B}$ and $T_f^{A/B}$ being the enthalpies and temperatures of fusion of the pure component phases *A* and *B*, respectively.

The expressions of $G^l$ and $G^s$ then become:

$$G^l(T,X_A^l) = RT[X_A^l \ln X_A^l + (1 - X_A^l)\ln(1 - X_A^l)] \quad [4]$$

$$G^s(T,X_A^s) = X_A^s \Delta H_f^A \frac{T_f^A - T}{T_f^A} + (1 - X_A^s) \Delta H_f^B \frac{T_f^B - T}{T_f^B} + RT[X_A^s \ln X_A^s + (1 - X_A^S)\ln(1 - X_A^S)] + \Delta G_e^s \quad [5]$$

where $\Delta G_e^s = 0$ for an ideal solid solution, and $\Delta G_e^s$ is given by Equation 2 for a subregular solution.

The temperatures and heats of fusion of the pure components are known (1,2,8). The interaction parameters $\Omega_{AB}$ and $\Omega_{BA}$ that appear in the subregular solution have to be determined. A calculation at each temperature *T* of the common tangent of the curves $G^s(T,X_A)$ and $G^l(T,X_A)$ (i.e., same chemical potential in the two phases for each component) gives the equilibrium composition of the two phases (liquidus and solidus), and thus the composition domain where liquid and solid are present together in equilibrium (16). To obtain the theoretical solid–liquid phase diagrams, this process was repeated for all temperatures with a unique set of $\Omega_{AB}$, $\Omega_{BA}$ values. $\Omega_{AB}$ and $\Omega_{BA}$ were used as adjustable parameters to fit the theoretical phase diagrams to the experimental points.

*Crystallization kinetics*. To study solidification kinetics, a series of DSC isothermal experiments (as described above) were performed for three compositions of the POS–SOS system: 25:75, 50:50, and 75:25. For each composition and $T_{iso}$ the evolution of the volume fraction of solid, $f_s(t)$, was obtained by numerical integration of the DSC exothermal peaks of solidification, after correction for the baseline. From the evolution of $f_s(t)$, two parameters were calculated for further analysis: the time of onset, $t_{onset}$, and the time of finish, $t_f$, of the transformation, which correspond to $f_s(t_{onset}) = 1\%$ and $f_s(t_f) = 99\%$, respectively. TTT diagrams, which represent the phase transformation kinetics under isothermal conditions, were also constructed, as previously described (8): for each isothermal solidification plateau, $t_{onset}$ and $t_f$ of the phase transformation were reported on the diagram, thus delimiting the time domain when liquid and solid coexist. For each experiment on the FP900 apparatus, the morphology and evolution of the crystals that formed on the isothermal plateau also were observed. Maps of crystal morphology as a function of the temperature of solidification were then constructed for the three compositions. When the crystals were sufficiently large spherulites (>10–20 $\mu$m), growth rate of the solid–liquid interface, *v*, was estimated from the slope of the evolution of the spherulite radius with time, averaged over at least 20 different grains. *v* was then displayed as a function of undercooling, ΔT (i.e., the departure of temperature from equilibrium).

As for pure TAG (8), a model, based on the data from the isothermal experiments and simulating the crystallization kinetics during continuous cooling, was applied to the binary system POS–SOS 25:75. A finite element code was used to calculate the evolution of temperature in the DSC sample, knowing the physical properties of the material and the initial and boundary conditions. This calculation was coupled with a microscopic model of crystallization, which uses an additivity principle and the isothermal data to simulate the solidi-

fication path at any node of the finite element mesh (17). For this purpose, the corresponding cooling curve was decomposed into small steps, during which the temperature was held constant and isothermal solidification data could be used to estimate the evolution of the solid fraction. As a result, evolution of the fraction of each phase in the sample can be calculated. Predictions of the model were compared with experimental results obtained on the DSC7 apparatus. Starting from a completely liquid state at 100°C, the sample was quickly cooled at 50°C/min to 35°C. Then, from 35°C, the cooling rate was changed to the desired value, between 0.5 and 5°C/min, and the sample was cooled until it reached 15°C. During this stage, the sample solidified, and from the integration of the DSC peaks of the phase transformations, the evolution of the global latent heat was obtained. Finally, as for the isothermal experiments, the sample was reheated at 5°C/min for identification and determination of the proportion of the phases formed.

## RESULTS AND DISCUSSION

*Thermodynamic properties—binary diagram.* Thermodynamic characteristics of the various solid structures observed in the POS–SOS system are reported as binary phase diagrams in Figure 1. The $\Delta H_f$ of the phases are plotted as a function of composition in Figure 2. For the sake of clarity, the stable ($\beta_1$) and metastable ($\beta_2$, $\beta'$ and $\delta$, $\alpha$ and sub-$\alpha$) phase diagrams are shown separately (Figs. 1A–1D). For each composition, two points are represented in the diagrams, the filled one is the solidus temperature, i.e., the temperature at which some liquid starts to appear on remelting, the open one is the liquidus, i.e., the temperature at which the last solid melts. As explained in the Materials and Methods section, the various phases observed were identified with the help of the $\Delta H_f$, shown in Figure 2, and of the melting ranges. These values were compared with those of the pure TAG. The value of the $\Delta H_f$ was particularly useful because it follows quite accurately a linear rule of mixture. As in our preceding study (8), the denomination of Sato *et al.* (1,2) was used for the phases of the TAG with the possible addition of the chainlength structure after the symbol of the phase (i.e., β-3 is phase β with a triple chainlength structure).

The stable phase β was found as one form in POS, β-3, and two forms in SOS, $\beta_1$-3 and $\beta_2$-3. Compared with the values of other authors (1–3,6,7), the $T_f$ and the $\Delta H_f$ of these phases found in the present work were similar (18). For the system POS–SOS, the β phase seems to be a solid solution with complete miscibility at all temperatures. However, the most-stable form of SOS, $\beta_1$-3, was not obtained on the SOS-rich side of the diagram. The values reported in Figure 1A are those of Wesdorp (6): they indicate a solid solution between β-3(POS) and $\beta_1$-3(SOS). In the present experiments, a solid solution between β-3(POS) and $\beta_2$-3(SOS) was observed (Fig. 1B). In both Figures 1A and 1B, the theoretical subregular solution curve was fitted to the experimental points (parameters of the models shown in Table 1). For [β-3 (POS),$\beta_2$-3(SOS)] (Fig.

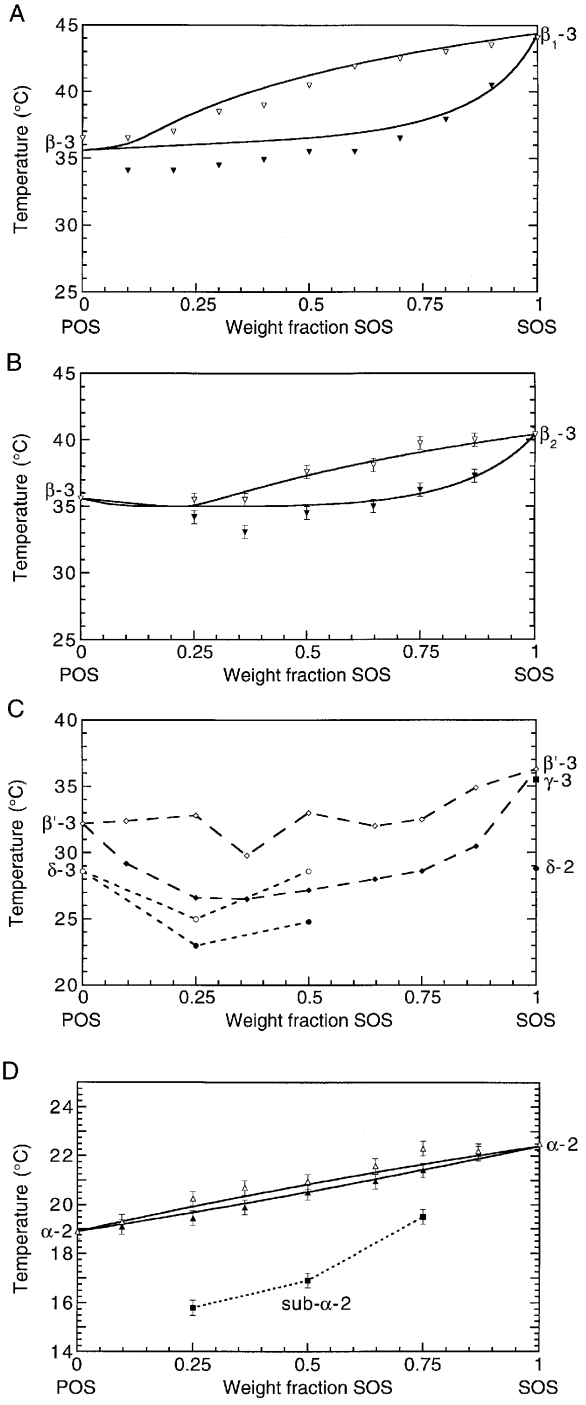


**FIG. 1.** Phase diagram of: (A) β-3[1-palmitoyl-2-oleoyl-3-stearoyl-*sn*-glycerol(POS)] and $\beta_1$-3[1,3-distearoyl-2-oleoyl-*sn*-glycerol(SOS)]; (B) β-3(POS) and $\beta_2$-3(SOS); (C) β′-3(POS) and β′-3(SOS), δ-3(POS) and δ-2(SOS); (D) α-2(POS) and α-2(SOS) and sub-α. Markers represent experimental points [from Wesdorp (6) in A]. In A and B, the continuous curves are the theoretical equilibrium liquidus and solidus for ideal liquid and subregular solid solutions. In D, the continuous curves correspond to the theoretical curves for ideal solutions of the liquid and α.

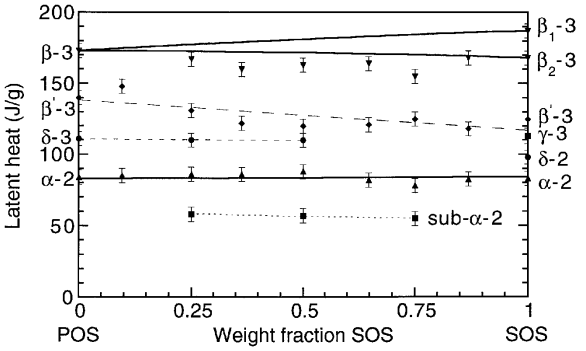


**FIG. 2.** Latent heat of fusion of the phases observed for different compositions of the binary system POS–SOS. Continuous curves correspond to the theoretical values of the α ideal solution and β subregular solutions. See Figure 1 for abbreviations.

1B), the fitted liquidus and solidus curves seem to indicate an azeotrope at about 25% SOS. In the domain 0–25% SOS, the zone of solid–liquid equilibrium (solidification interval) is narrow. Unfortunately, a stable form of SOS–POS 10:90 was never observed to support this. The full miscibility and compatibility of POS and SOS in a β structure are supported by X-ray diffraction, Fourier transform infrared spectroscopy, and solid nuclear magnetic resonance experiments (4,5), which indicate that the crystalline structures of the β phases of the two species are almost identical.

Results for the intermediate phases were more difficult to interpret because several phases with close melting ranges could be present simultaneously. Nevertheless, it appears that two different phases, δ and β′, whose data points are shown in Figure 1C, could be identified from the experiments. They could be separated because the first phase, identified as δ, had a $\Delta H_f$ of about 100–110 J/g, while the second one, presumably β′, had a $\Delta H_f$ between 120 and 140 J/g. The second was assumed not to be γ because it was not observed for POS. δ(SOS), denominated $\beta'_2$-2 by Culot (19), has a double-layer structure, while δ-3(POS) has a triple-layer structure. For compositions higher than 50% in SOS, δ was not observed, and β′ formed directly. This shows a noncompatibility of the two phases δ-3(POS) and δ-2(SOS), reason why the diagram of δ-3(POS) was not extended on the SOS side. Furthermore, no theoretical curve could be fitted to the δ and β′ experimental points. This is probably due to the fact that, unlike the stable phase β, δ and β′ were formed transitorily over short periods of time; thus a complete state of equilibrium of the solid is not guaranteed, and thus the exactitude of the liquidus line. Yet, β′ seems to be a solid solution with a minimum around 30–40 wt% SOS.

Figure 1D shows the phase diagram of the least-stable phases. For pure POS and SOS, α is the least-stable phase to form (triangles). Its $\Delta H_f$ could be measured with good accuracy, due to its presence alone. The values, between 80 and 85 J/g (see Table 1), are in agreement with earlier data (6,7). The seven compositions studied between pure POS and pure SOS all exhibited an α phase. Figure 1D shows that the experimental points can be approximated quite well by the ideal α-solution curve (see Table 1 for the parameters used in the model). This confirms the results of Wesdorp (6), which show an ideal behavior for the α phase of binary systems of TAG with similar fatty acid chainlengths. With the DSC7 apparatus, another less-stable phase (filled squares), with a lower melting temperature and $\Delta H_f$ than those of α, was found for the mixtures. According to the literature (7,19), this phase, which we never observed for pure POS and SOS, would be sub-α. The peak on remelting is narrow, and therefore, only one point is shown in Figure 1D for sub-α.

*TTT diagrams and morphologies of the grains.* Kinetics studies were performed for three compositions of POS–SOS, 25:75, 50:50 and 75:25. As previously done for the three pure TAG POP, POS and SOS (8,20), results are presented as TTT diagrams and morphology maps. Figures 3 and 4 show the three TTT diagrams, measured with the FP900 and DSC7, respectively. The gray zones in these figures outline the solidus–liquidus regions, i.e., the MR, of the various phases. Figure 5 gives the grain morphologies and phases observed for the three mixtures with the FP900 apparatus as a function of the temperature of the isothermal solidification. Results obtained with the two instruments did not differ significantly, except for slightly faster kinetics in the glass pans of the FP900. This behavior, already observed with the pure TAG (8), was more pronounced for the most-stable phases. Due to its slow rate of crystallization, the stable β-phase was not observed in these kinetics studies. Moreover, the most metastable phase sub-α was not observed with the FP900 because, in its temperature range of formation, the kinetics of solidification were too fast to be observed correctly.

*POS–SOS 75:25 (Figs. 3A, 4A, 5A).* Three phases were identified: sub-α was the least stable and appeared quickly at the lowest temperatures with the DSC7. It retransformed almost immediately into α. The α phase formed over a fairly large temperature range. Just below the MR of α, another phase, δ, appeared together with α, whereas above it, δ formed alone. The crystals appeared like a fine mass uniformly in the volume, except at the highest temperatures, where the structure of δ became coarser and the spherulites became visible.

**TABLE 1**
**Parameters Used for Theoretical Calculations of the Phase Diagrams**

| Phases | Parameter[a] | POS | SOS |
|---|---|---|---|
| α(POS)–α(SOS) | $T_f$ | 18.9°C | 22.4°C |
| | $\Delta H_f$ | 83 J/g | 84 J/g |
| β(POS)–$\beta_2$(SOS) | $T_f$ | 35.6°C | 40.4°C |
| | $\Delta H_f$ | 173 J/g | 168 J/g |
| | $\Omega_{AB}$, $\Omega_{BA}$ | 1.2 | 2 |
| β(POS)–$\beta_1$(SOS) | $T_f$ | 35.6°C | 44.4°C |
| | $\Delta H_f$ | 173 J/g | 187 J/g |
| | $\Omega_{AB}$, $\Omega_{BA}$ | 1.1 | 1.5 |

[a] $T_f$ and $\Delta H_f$ are the temperature and the heat of fusion, respectively. $\Omega_{AB}$ and $\Omega_{BA}$ are the parameters of the subregular model for the solid phase, determined from fitting the theoretical equilibrium curves to the experimental points. POS, 1-palmitoyl-2-oleoyl-3-stearoyl-*sn*-glycerol; SOS, 1,3-distearoyl-2-oleoyl-*sn*-glycerol.

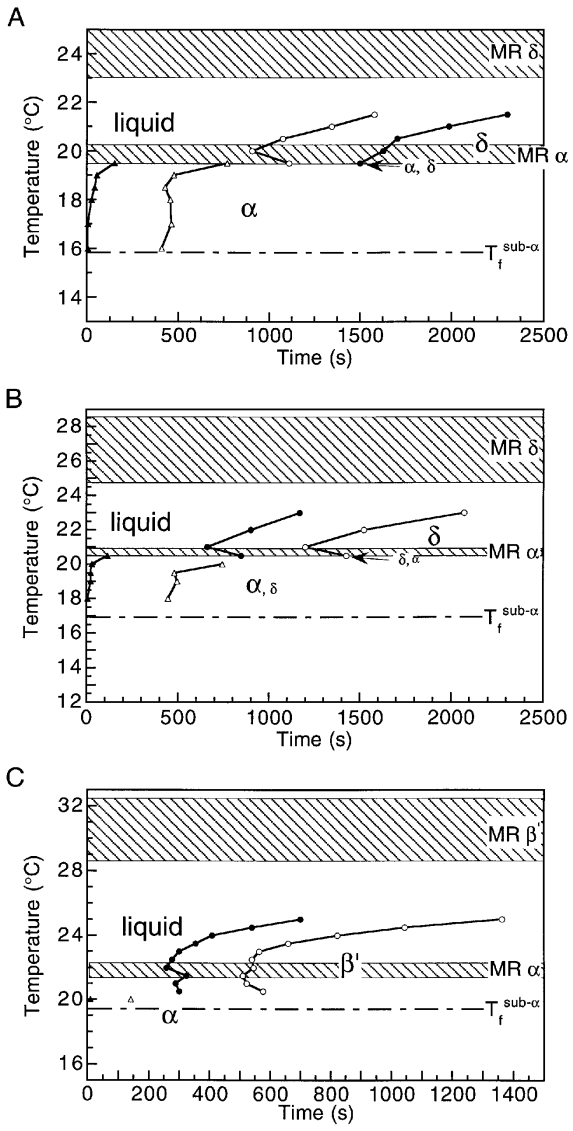


**FIG. 3.** Time–temperature–transformation (TTT) diagrams constructed from the FP900 experiments: (A) POS–SOS 75:25; (B) POS–SOS 50:50; (C) POS–SOS 25:75. Filled and open symbols correspond to the onset time and the finish time of the transformation, respectively. Hatched areas correspond to melting ranges (MR) of the various phases observed. See Figure 1 for other abbreviations.

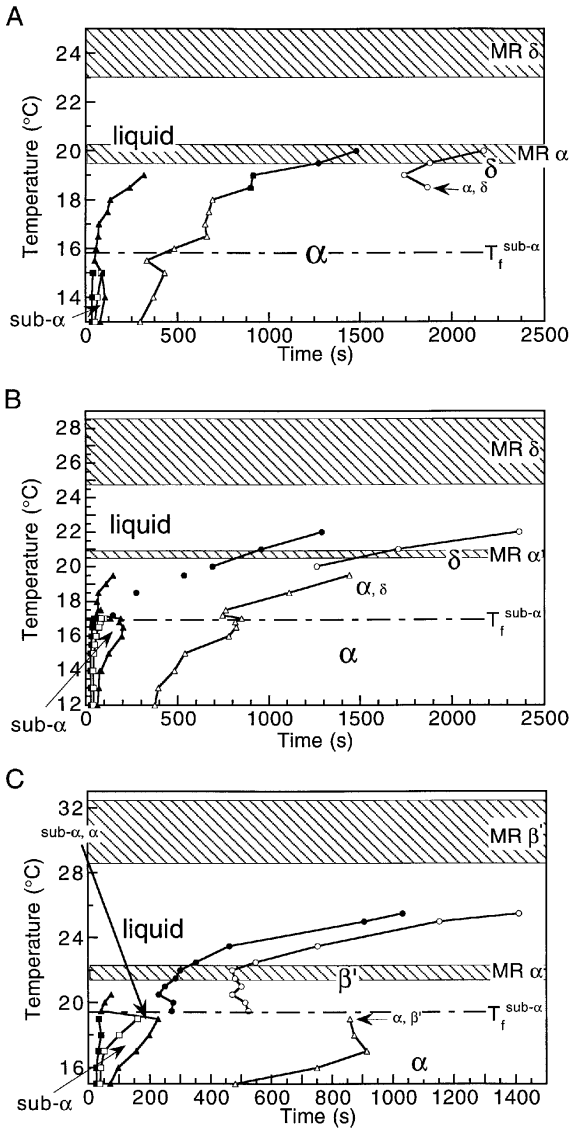


**FIG. 4.** TTT diagrams constructed from the DSC7 experiments: (A) POS–SOS 75:25; (B) POS–SOS 50:50; (C) POS–SOS 25:75. Abbreviations as in Figures 1 and 3.

*POS–SOS 50:50 (Figs. 3B, 4B, 5B).* The observations are similar to those made for the POS–SOS 75:25 system. At low temperatures, sub-α, observed only with the DSC7, retransformed almost immediately into α. In the upper part of the domain of α, a small quantity of δ formed, whereas above, only δ formed. The α form was only present as a very dispersed phase. The structure of δ was also a dispersed phase of small crystals, which became coarser with an increasing solidification temperature, and above 21.5°C, spherulites were visible under the microscope.

*POS–SOS 25:75 (Figs. 3C, 4C, 5C).* For this composition, three domains delimit the presence of three single phases, sub-α, α and β′. Below 19.5°C, sub-α formed with the DSC7 and then retransformed into α. Contrary to the other compositions, δ was not observed. At about 20°C, α started to form, but then the solidification of β′ occurred, and no more α was found at the end of the plateau (Fig. 4C). Above 20°C, only β′ crystallized. α appeared as small dispersed crystals forming a fine mass. β′ also formed as a fine dispersed mass below 22.5°C, but it had a coarser structure with visible spherulites above this temperature. Beyond 24°C, a directional mass of

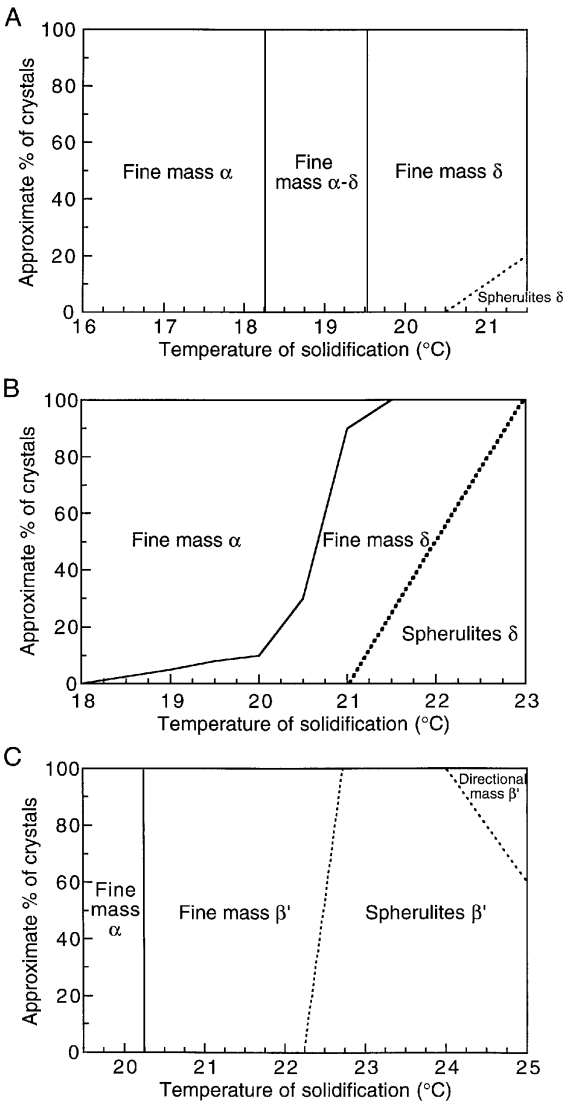


**FIG. 5**. Approximate volume fractions of the various grain morphologies and crystalline phases for: (A) POS–SOS 75:25; (B) POS–SOS 50:50; (C) POS–SOS 25:75. See Figure 1 for abbreviations.

β′ growing from the outer sample appeared, as in the case of pure SOS (8).

*Evolution of crystallization kinetics with composition.* From the TTT diagrams obtained with the DSC7 apparatus for the three binary systems and for POS and SOS [from Ref. (8)], the change in crystallization kinetics with SOS composition of the equivalent phases was investigated. Figures 6 and 7 show, for each composition and for each group of phases, sub-α, α and δ/γ/β′, the temperature of solidification as a function of the onset time (i.e., induction time) and the finish time of crystallization, respectively. No points are reported in Figs. 6A and 7A for pure POS and SOS because sub-α was not observed in these products. Moreover, no finish time corresponding to the liquid→α transformation of the 25:75 mixture is reported in Figure 7B because the transformation was overcome by liquid → δ and α → δ before the end. For a given temperature, an increasing percentage of POS in general delayed the start (Fig. 6) and finish (Fig. 7) of crystallization and increased the solidification duration, i.e., $t_f - t_{onset}$. α-SOS is an exception: it exhibited a surprisingly high induction time (Fig. 6B) but a fairly fast kinetics once nucleation had occurred (Fig. 7B). The induction time of SOS δ and γ phases was close to that of POS–SOS 25:75 (Fig. 6C), but the crystallization was again faster (Fig. 7C). The delayed onset of α-crystallization of pure SOS, compared to the mixtures, is yet unexplained. However, for all phases, once nucleation had started, the overall solidification of SOS was faster, compared to that of the mixtures. To confirm these observations, the growth rate of the solid–liquid interface of sufficiently large spherulites was measured as a function of the undercooling for the δ/γ/β′ phases of the three mixtures and of pure POS and SOS (see Fig. 8). Undercooling ΔT is defined as the difference between the liquidus temperature of the phase diagram and the isothermal temperature at which crystallization occurs. At a given undercooling, δ-SOS has a growth rate that is nearly one order of magnitude higher than that of the binary mixtures or POS. POS seems to act as a "brake" to crystallization, probably due to asymmetry of its molecule. Indeed, asymmetric molecules need more time to attach in the right position to the solid phase, thus slowing down the attachment kinetics.

*Modeling of continuous cooling.* In the DSC7 apparatus, a sample of the binary composition POS–SOS 25:75 was cooled from 35 to 15°C at four different rates: 0.5, 1, 2, and 5°C/min. Crystallization kinetics were then compared with predictions from the model described in the Materials and Methods section. The sample, at first completely liquid, solidified into different solid phases depending on the cooling conditions. From the model, it appears that, even at 5°C/min, the temperature in the DSC pan is almost homogeneous, and so are the phase fraction distributions. The experimental and simulation results were compared as a function of the cooling rate: the times of onset and finish of phase transformation are reported in Figure 9, and the final proportions of the different solid phases formed are shown in Figure 10. The times of onset and finish decreased with increasing cooling rate, because the undercooling (i.e., the driving force of the transformation) increased more rapidly, and also more metastable phases formed. The model gives a fairly good estimation of these two times. Phase proportions are also well predicted. At 0.5°C/min, β′ had enough time to nucleate and grow before the other metastable phases appeared. At higher cooling rates, β′ was less and less present at the expense of α and sub-α. At 1°C/min, α and sub-α were present in equivalent proportions, but at 2 or 5°C/min, almost only the most metastable phase sub-α formed. The high sensitivity of phase formation to the cooling conditions is well-reproduced by the model based on TTT diagrams and an additivity principle.

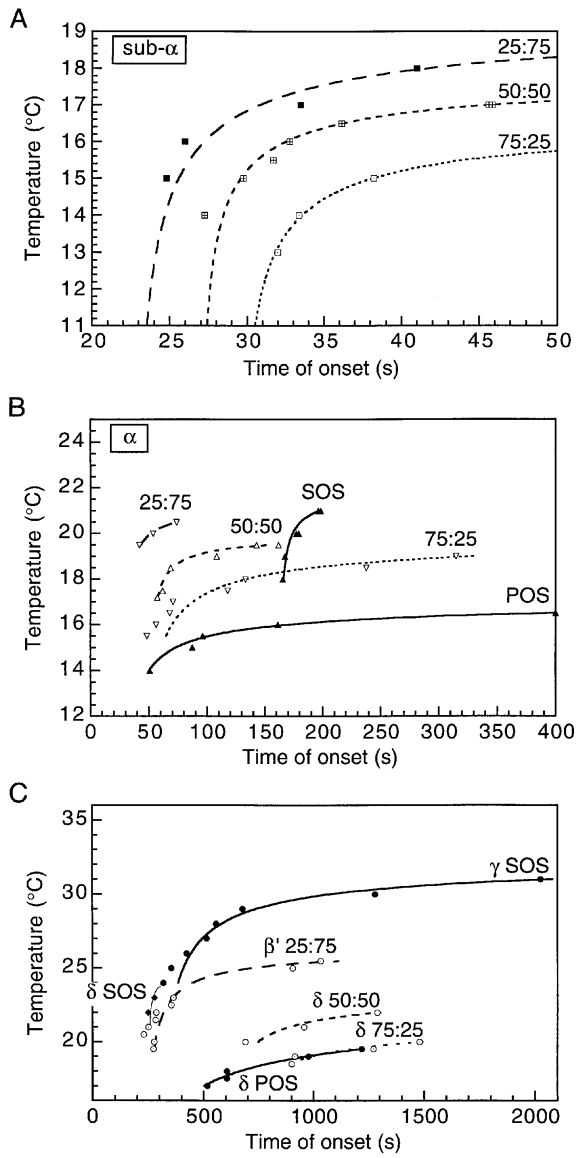


**FIG. 6.** Temperature of solidification as a function of the onset time (i.e., induction time) of the transformation for the binary POS–SOS mixtures solidifying as: (A) sub-α; (B) α; (C) δ/γ/β′. See Figure 1 for abbreviations.

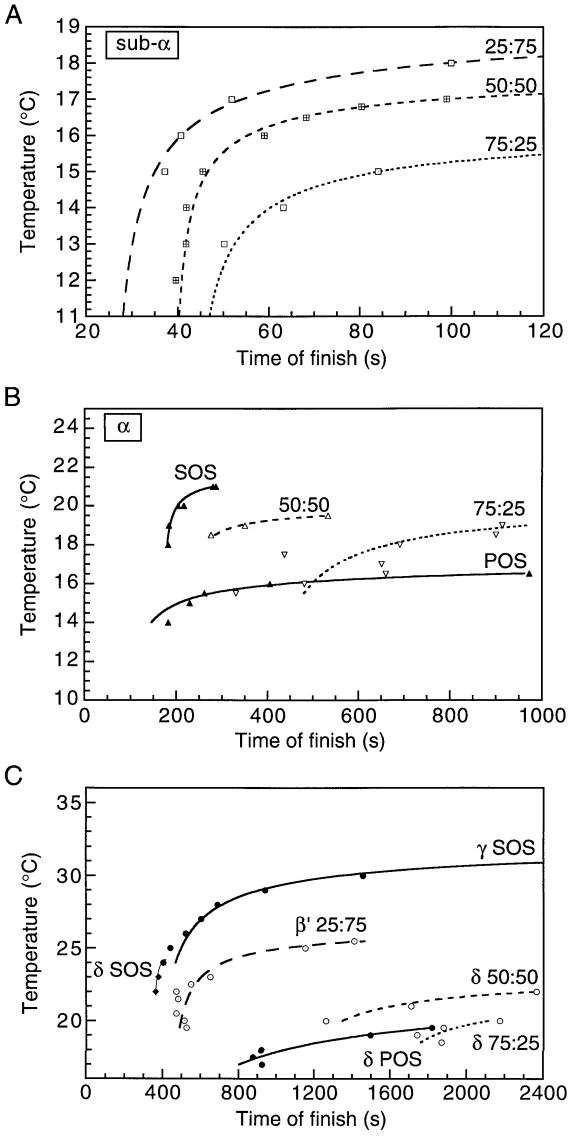


**FIG. 7.** Temperature of solidification as a function of the finish time of the transformation for the binary POS–SOS mixtures solidifying as: (A) sub-α; (B) α; (C) δ/γ/β′. See Figure 1 for abbreviations.

## ACKNOWLEDGMENTS

The authors thank the Commission pour la Technologie et l'Innovation (CTI), Bern, Switzerland, and the Nestlé Research Center, Verschez-les-Blanc, Switzerland, for their financial support (CTI project 2944.1). The encouragement of Dr. J. Löliger and helpful discussions with Dr. C. Bertoli from the Nestlé Research Center are also gratefully acknowledged.

## REFERENCES

1. Sato, K., T. Arishima, Z.H. Wang, K. Ojima, N. Sagi, and H. Mori, Polymorphism of POP and SOS. I. Occurrence and Polymorphic Transformation, *J. Am. Oil Chem. Soc. 66*:664–674 (1989).
2. Arishima, T., N. Sagi, H. Mori, and K. Sato, Polymorphism of POS. I. Occurrence of Polymorphic Transformation, *Ibid. 68*:710–715 (1991).
3. Arishima, T., and K. Sato, Polymorphism of POP and SOS. III. Solvent Crystallization of β2 and β1 Polymorphs, *Ibid. 66*:1614–1617 (1989).
4. Yano, J., K. Sato, T. Arishima, N. Sagi, F. Kaneko, and M. Kobayashi, FT–IR Study of Polymorphic Transformations in SOS, POP and POS, *J. Phys. Chem. 97*, 12967–12973 (1993).
5. Arishima, T., K. Sugimoto, R. Kiwata, H. Mori, and K. Sato, $^{13}C$ Cross-Polarization and Magic-Angle Spinning Nuclear

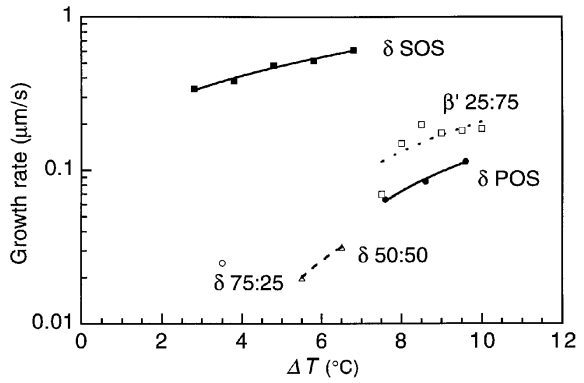


**FIG. 8.** Growth rate of spherulites of the most-stable phase observed as a function of the undercooling, for five compositions of the binary system POS–SOS. See Figure 1 for abbreviations.

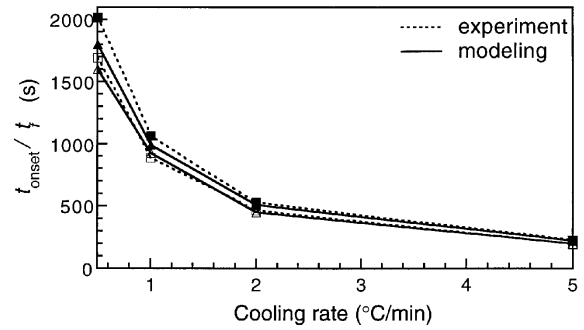


**FIG. 9.** Simulated (continuous lines, triangles) and experimental (dashed lines, squares) onset (empty symbols), and finish (filled symbols) times as a function of the cooling rate for the POS–SOS 25:75 mixture. See Figure 1 for abbreviations.

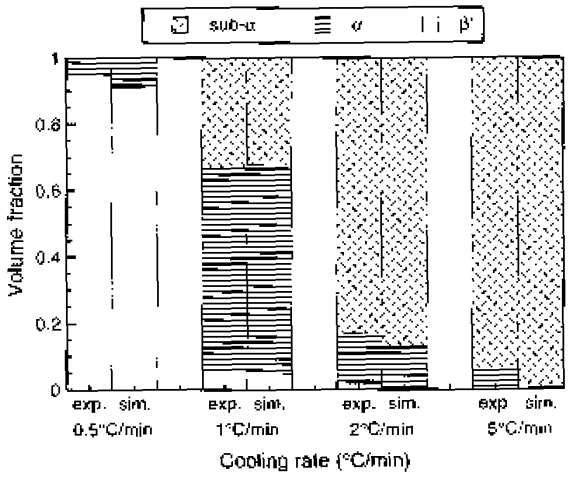


**FIG. 10.** Simulated and experimental fractions of phases formed as a function of the cooling rate for the POS–SOS 25:75 mixture. See Figure 1 for abbreviations.

Magnetic Resonance of Polymorphic Forms of Three Triacylglycerols, *J. Am. Oil Chem. Soc. 73*:1231–1236 (1996).
6. Wesdorp, L., Liquid-Multiple Solid Phase Equilibria in Fats—Theory and Experiments, Ph.D. Thesis, Technical University of Delft, The Netherlands, 1990.
7. Cebula, D., and K. Smith, Differential Scanning Calorimetry of Confectionery Fats. Pure Triglycerides: Effects of Cooling and Heating Rate Variation, *J. Am. Oil Chem. Soc. 68*:591–595 (1991).
8. Rousset, Ph., and M. Rappaz, Crystallization Kinetics of the Pure Triacylglycerols Glycerol-1,3-Dipalmitate-2-Oleate, Glycerol-1-Palmitate-2-Oleate-3-Stearate, and Glycerol-1,3-Distearate-2-Oleate, *Ibid. 73*:1051–1057 (1996).
9. Koyano, T., I. Hachiya, T. Arishima, N. Sagi, and K. Sato, Polymorphism of POS. II. Kinetics of Melt Crystallization, *Ibid. 68*:716–718 (1991).
10. Koyano, T., I. Hachiya, T. Arishima, K. Sato, and N. Sagi, Polymorphism of POP and SOS. II. Kinetics of Melt Crystallization, *Ibid. 66*:675–679 (1989).
11. Rossel, J.B., Phase Diagrams of Triglyceride Systems, *Adv. Lipid Res. 5*:353–408 (1967).
12. Wille, R., and E. Lutton, Polymorphism of Cocoa Butter, *Ibid. 43*:491–496 (1966).
13. Ollivon, M., and R. Perron, in *Manuel des Corps Gras*, Vol. 1, edited by A. Karleskind, Lavoisier, Paris, pp. 1992, 498–499.
14. Minato, A., S. Ueno, J. Yano, Z.H. Wang, H. Seto, Y. Amemiya, and K. Sato, Synchrotron Radiation X-Ray Diffraction Study on Phase Behavior of PPP–POP Binary Mixtures, *J. Am. Oil Chem. Soc. 73*:1567–1572 (1996).
15. Minato, A., S. Ueno, K. Smith, Y. Amemiya, and K. Sato, Thermodynamic and Kinetic Study on Phase Behavior of Binary Mixtures of POP and PPO Forming Molecular Compound Systems, *J. Phys. Chem. B 101*:3498–3505 (1997).
16. Lupis, C.H.P., *Chemical Thermodynamics of Materials*, Prentice-Hall PTR, New York, 1983.
17. Jacot, A., M. Swierkosz, J. Rappaz, M. Rappaz, and D. Mari, Modelling of Electromagnetic Heating, Cooling and Phase Transformations During Surface Hardening of Steels, *J. Physique 4(C1)*:203–213 (1996).
18. Rousset, Ph., Etude expérimentale et modélisation de la cristallisation de triacylglycérols et du beurre de cacao, Ph.D. Thesis 1718, EPFL Ecole Polytechnique Fédérale de Lausanne, Lausanne, 1997.
19. Culot, C., Modélisation du comportement polymorphique des triglycérides, Ph.D. Thesis, Université Notre Dame de la Paix, Namur, Belgium, 1994.
20. Rousset, Ph., and M. Rappaz, α-Melt-Mediated Crystallization of POS, *J. Am. Oil Chem. Soc. 74*:693–697 (1997).

[Received June 16, 1997; accepted February 11, 1998]